

Diffusion and jump-length distribution in liquid and amorphous $\text{Cu}_{33}\text{Zr}_{67}$

M. Kluge and H. R. Schober

Institut für Festkörperforschung, Forschungszentrum Jülich, D-52425, Germany

(Dated: November 21, 2018)

Using molecular dynamics simulation, we calculate the distribution of atomic jumps in $\text{Cu}_{33}\text{Zr}_{67}$ in the liquid and glassy states. In both states the distribution of jump lengths can be described by a temperature independent exponential of the length and an effective activation energy plus a contribution of elastic displacements at short distances. Upon cooling the contribution of shorter jumps dominates. No indication of an enhanced probability to jump over a nearest neighbor distance was found. We find a smooth transition from flow in the liquid to jumps in the glass. The correlation factor of the diffusion constant decreases with decreasing temperature, causing a drop of diffusion below the Arrhenius value, despite an apparent Arrhenius law for the jump probability.

PACS numbers: 61.43.Fs, 66.10.-x, 66.30.-h, 64.70.Pf

I. INTRODUCTION

Metallic glasses are of great interest both fundamentally and due to numerous applications. The absence of strong covalent bonds makes them the prime example of random dense packing. Atomic transport in metallic glasses and their melts is generally considered to be effected by two distinct mechanisms: flow in the liquid, and thermally activated hopping in the glassy state. See Ref. [1] for a review. When a glass forming liquid is cooled towards the glass transition diffusion drops faster than predicted by an Arrhenius law. The diffusion coefficient is often described by a Vogel-Fulcher law which can be rationalized e. g. by a free volume description. Mode coupling theory predicts for fragile glass formers, to which amorphous metallic alloys belong, a dynamical transition at a critical temperature, T_c , well above the glass transition temperature T_g . At T_c flow motion freezes and diffusion vanishes with a power law $D \propto (T - T_c)^\gamma$ apart from a residual contribution from atomic hopping². The mechanism of this change from flow to hopping is not understood.

In liquids with loose packing, flow is governed by binary collisions between the constituent atoms. In the undercooled melt, where the atomic packing is dense, flow is strongly collective. This is reflected in the observed small isotope effect of diffusion³, similar to the one observed earlier in the glassy state⁴. From these experiments it has been concluded that, both below and above the glass transition, diffusion is by collective motion of ten or more atoms. This poses the question of whether the change from flow to hopping is a change to a new elementary process or whether hopping evolves out of the flow motion.

Over the last few years computer simulations have provided considerable insight into the atomic dynamics of glasses and undercooled liquids. Early molecular dynamics simulations (MD) have shown collective jumps in undercooled liquids^{5,6}. Chains of atoms replacing each other were observed, i.e. the single atoms jumped by a nearest neighbor distance. These chains can close to form rings^{5,7}. Comparing successive configurations, averaged

over typical vibrational times, one again finds chain-like structures of atoms which have moved collectively in the undercooled liquid^{8,9,10}. These are not necessarily replacement chains. The jump process in the glassy state has been found to involve many atoms, each single atom moving only a fraction of the nearest neighbor distance in such a jump^{11,12,13}.

Upon cooling towards the glass-transition a striking feature is seen in the self-part of the van Hove function $G^s(r, t)$ which is related to the probability that an atom has moved by a distance r during a time t . At high temperatures $G^s(r, t)$ is perfectly Gaussian and broadens $\propto \sqrt{t}$. Upon cooling towards T_c , and beyond, a tail to larger distances grows with time. Finally approaching T_c an additional second peak at the nearest neighbor distance evolves, particularly for the more mobile components. This effect can be taken as one of the signatures of the glass transition¹⁴. From this behavior it was concluded that there is a single peaked distribution of hopping distances¹⁵. The time evolution of $G^s(r, t)$ in CuZr could be reproduced by a simple model involving jumps over nearest neighbor distances plus a residual small flow¹⁶. In this picture the jump motion dominates the diffusion in the undercooled liquid and the super-Arrhenius drop of diffusion stems from an increase of the return jump probability, as one would expect from an increasing number of blocked paths.

In a quantitative investigation of the deviation of $G^s(r, t)$ from a Gaussian, the non-Gaussianity parameter, $\alpha_2(T, t)$, was found to increase rapidly in the undercooled liquid but no abrupt change near T_c was seen^{17,18}. The time evolution could be understood from a model of collective jumps¹⁷.

Inspecting the pressure derivative of the diffusion constant, the apparent activation volume, one finds a strong cusp at T_c which could indicate a change of diffusion mechanism¹⁹.

These different findings pose the question of whether there is a change in the elementary process of diffusion near T_c , in particular whether one might observe the evolution of a typical jump process in the glass.

II. SIMULATION DETAILS

Here we report a MD investigation of the atomic jump lengths in undercooled and glassy $\text{Zr}_{67}\text{Cu}_{33}$. For the inter-atomic interaction we use a modified Embedded Atom Method.²⁰ The parameters were fitted to reproduce the experimental values of Cu, Zr and CuZr_2 crystals. The universal energy-volume relation of Rose *et al.*²¹ was used to determine the anharmonic contributions, not sampled in the crystal but of essential importance in the disordered glassy state. We get lattice parameters $a = 0.363$, $a = 0.323$, $c = 0.516$ and $a = 0.338$, $c = 10.35$ nm (experimental values²² $a = 0.362$, $a = 0.323$, $c = 0.515$ and $a = 0.322$, $c = 11.18$ nm) for Cu, Zr and CuZr_2 , respectively. The CuZr_2 lattice is slightly distorted. The atomic volume, however, is only 2% too large. The sublimation energies for Cu and Zr (3.53 and 6.34 eV) agree with experiment. We find enthalpies of fusion per atom relative to the mono-atomic crystalline phases at room temperature of $\Delta_f H = 0.22$ and 0.18 eV (experiment²³ for CuZr_2 and CuZr , respectively). The vacancy formation energies are 1.32 and 1.63 eV (experiment²⁴ 1.28 and > 1.5 eV) for Cu and Zr, respectively. Additionally the phonon dispersion curves and elastic constants of the mono-atomic lattices were used. In the case of Cu excellent agreement was achieved. In Zr we get an overall agreement with experiment but some phonons deviate up to 30%, similar to other work^{25,26}. No attempt was made to fine tune the potential to fully reproduce the phase diagram. The detailed form and the parameters are given in the appendix. For more details on the fitting procedure see Ref.²⁷.

The MD calculations were done using the velocity Verlet algorithm with a time-step of $2.5 \cdot 10^{-15}$ s and systems of $N = N^{\text{Zr}} + N^{\text{Cu}} = 1000$ atoms with periodic boundary conditions. Previous work on other systems (e. g. soft spheres, binary Lennard-Jones, Se) by us and other groups has shown that this size suffices to reproduce the dynamics at elevated temperatures. As additional test some runs with $N = 8000$ were done for comparison. For the questions investigated in this work long aging times are more important than large system sizes. The pressure was kept constant following Ref.²⁸ using a volume mass of $\approx \sqrt{N} \cdot m_{\text{Zr}}$ and an additional damping term to prevent oscillations. Temperature was controlled by a Nosé-thermostat following Hoover²⁹.

Three independent samples were prepared by a quench from the hot liquid and were aged in intermittent stages, as shown in Fig. 1. We cool, in steps of 100 K, with a rate of 10^{12} K/s from 2000 K to the simulation temperature. At each temperature step the samples were aged for times ranging from 1 ns at 2000 K to 2 ns for $T \leq 1000$ K, before continuing the quench. The effective cooling rate was thus lowered by about an order of magnitude, compared to a straight quench with a constant rate. Before the actual measurements at a given temperature the systems were additionally aged at constant T for different

times, up to 5.5 ns, as indicated by the dotted lines in Fig. 1.

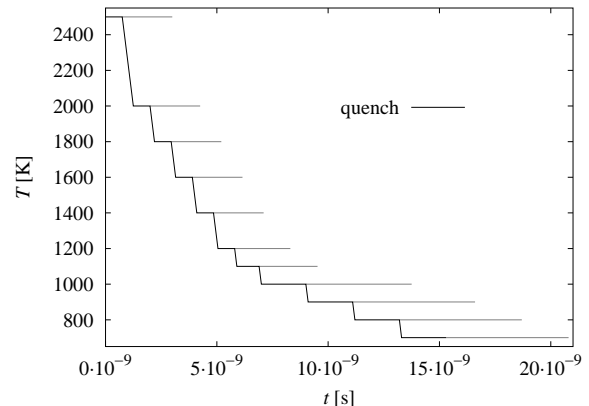


FIG. 1: Quench history of the samples (solid line). The dotted lines show the lengths of additional aging before the start of the measuring runs.

III. GLASS TRANSITION AND AGING

Experimentally $\text{Zr}_{67}\text{Cu}_{33}$ is a good glass-former, which melts at 1310 K³⁰ and can be under-cooled by a few hundred Kelvin. The experimental glass-transition temperature varies from 600 K at cooling-rates of 0.01 K/s to 750 K at 10^6 K/s³⁰. To determine the glass transition temperature of our CuZr model we did additional runs without the intermittent aging and monitored the potential energy and the volume as function of temperature for different quench rates, ranging from $Q = 2.5 \cdot 10^{13}$ K/s to $Q = 4 \cdot 10^{10}$ K/s, see Fig. 2 for the potential energy. The glass transition temperature, T_g , was defined by the crossover from the low temperature to the liquid behavior. In the limited range of Q covered by the simulation the dependence of T_g on Q can be expressed by a logarithmic law³¹

$$T_g = (463 + 20.6 \cdot \ln Q) \text{ K}. \quad (1)$$

For our lowest quench rate $Q = 4 \cdot 10^{10}$ K/s we find $T_g = 965$ K extrapolating to $Q = 4 \cdot 10^6$ K/s Eq. 1 gives $T_g = 747$ K in excellent agreement with the experimental value.

From Fig. 2 together with Eq. 1 we find a linear dependence of the average potential energy per atom at $T = 0$ on the glass transition temperature

$$E_p(T = 0, Q) = (-5.7715 + 1.5 \cdot 10^{-4} T_g(Q)) \text{ eV}. \quad (2)$$

Such a linear equation was also observed in amorphous Se for both energy and atomic volume³². In CuZr the quench rate dependence of the volume is too small to be evaluated.

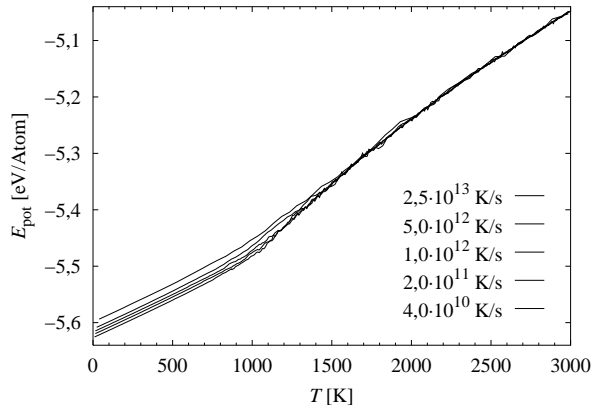


FIG. 2: Average potential energy per atom as function of temperature for different quench rates: from top to bottom $Q = 2.5 \cdot 10^{13}$, $5 \cdot 10^{12}$, $1 \cdot 10^{12}$, $2 \cdot 10^{11}$ and $4 \cdot 10^{10}$ K/s.

Monitoring the average potential energy per atom at $T = 1000$ K, near the glass transition temperature, starting at the end of the quench, Fig. 1, we find that it drops in 35 ns by about 0.014 eV. The statistics is not sufficient to determine the decay law unambiguously.

IV. DIFFUSION AND HETEROGENEITY

The average atomic mean square displacements (msqd), from the respective configurations after aging, are shown in Fig. 3 in a double logarithmic plot. For short times one observes an increase $\propto t^2$ which is typical for vibrational and ballistic motion. For long times the msqd increases $\propto t$, indicative of long range diffusion. Lowering the temperatures below $T = 1400$ K the plateau, typical for the undercooled liquid and the glass, evolves between these two limits. This onset of the plateau correlates well with the experimental melting temperature $T_m = 1310$ K³⁰. At the lowest temperatures, in the ps range, one can just see some small wiggles which reflect the vibration spectrum.

The diffusion coefficients of the two components, Fig. 4, were calculated in the usual way from the slope of the long time limit of the msqd. Fitting the diffusion coefficients in the undercooled melt according to MCT,

$$D_{\text{MCT}}(T) = D_0^{\text{MCT}} / (T - T_c)^\gamma, \quad (3)$$

we find $T_c = 1025$ K and $\gamma = 1.92$ and 1.34 for Zr and Cu, respectively. A fit to the relaxation time of the intermediate scattering function with the same T_c gives slightly higher values $\gamma = 2.2$ and 1.57 for Zr and Cu, respectively^{1,33}. These numbers are meant as a guide to the relevant temperatures and are not exact. An alternative fit with the Vogel-Fulcher-Tammann (VFT) relation

$$D_{\text{VFT}}(T) = D_0^{\text{VFT}} \exp(-E^{\text{VFT}}/k(T - T^{\text{VFT}})) \quad (4)$$

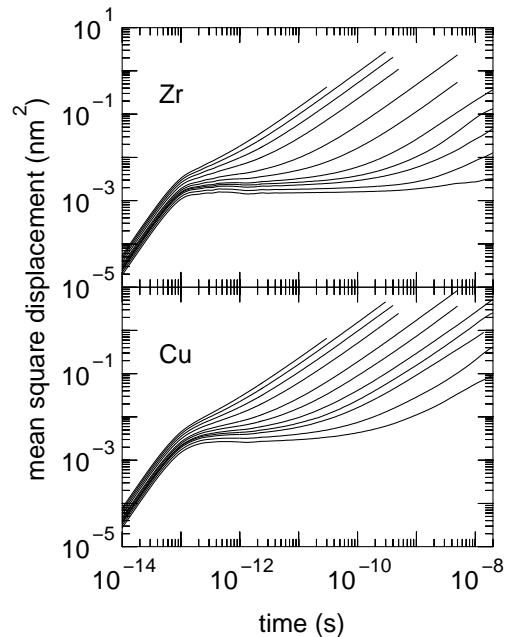


FIG. 3: Average mean square displacement as function of time on a double logarithmic scale. Temperature from top to bottom: 2000, 1800, 1600, 1400, 1200, 1100, 1000, 960, 900, 800, 700 K.

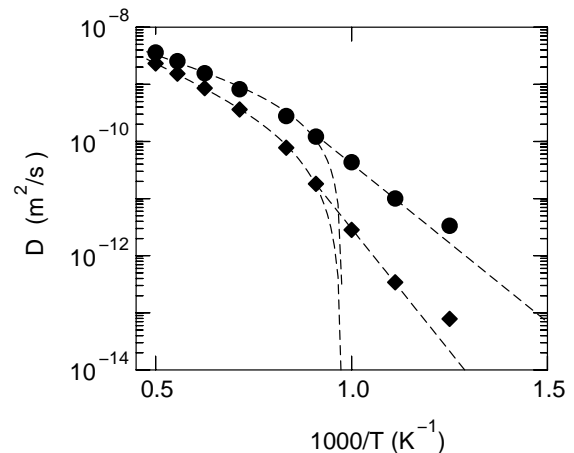


FIG. 4: Diffusion coefficients in $\text{Zr}_{67}\text{Cu}_{33}$ (Zr: diamonds, Cu: spheres) The dashed lines represent a fit with MCT, using the same temperature T_c for both components, in the undercooled melt and an Arrhenius fit in the glass.

gives for Zr $D_0^{\text{VFT}} = 2.65 \cdot 10^{-8}$ m²/s, $E^{\text{VFT}} = 0.28$ eV, $T^{\text{VFT}} = 641$ K and for Cu $D_0^{\text{VFT}} = 3.70 \cdot 10^{-8}$ m²/s, $E^{\text{VFT}} = 0.30$ eV, $T^{\text{VFT}} = 477$ K. In the glass the diffusivity can be described by the usual Arrhenius law

$$D_{\text{Arrh}}(T) = D_0^{\text{Arrh}} \exp(-E^{\text{m}}/kT). \quad (5)$$

Neglecting the values at $T = 800$ K, which are proba-

bly too high due to too short aging, we obtain $D_0^{\text{Arrh}} = 1.09 \cdot 10^{-3} \text{ m}^2/\text{s}$, $E^{\text{m}} = 1.7 \text{ eV}$, for Zr and $D_0^{\text{Arrh}} = 1.41 \cdot 10^{-5} \text{ m}^2/\text{s}$, $E^{\text{m}} = 1.1 \text{ eV}$, for Cu. Due to the small fitting range there is a considerable margin of error on these values. The deviation of the present values from the ones reported earlier by Gaukel²⁷ is due to the much improved statistics and aging of the present work. It should further be noted that fits in the undercooled liquid using the VFT or MCT expression is strongly influenced by the range of temperatures included in the fit. Furthermore in the fits of the previous work different values of T_c were allowed for Cu and Zr, respectively, whereas in the present work the condition of a unique value T_c was imposed. The data do not suffice to validate or invalidate this condition.

Including the 800 K values the activation energies would be considerably smaller ($E^{\text{m}} = 0.99$ and 0.75 eV for Zr and Cu, respectively^{1,33}).

Our results agree well with simulations of the similar NiZr system where a totally different model for the inter-atomic interaction was used³⁴. The diffusion coefficients of the two components both in NiZr and in a binary Lennard-Jones¹⁹ glass at zero pressure are nearly parallel in the melt, whereas in $\text{Zr}_{67}\text{Cu}_{33}$ they diverge. This effect is probably due to the weaker coupling between the two components in CuZr. Experimentally this is reflected in lower enthalpy of fusion in CuZr ²³ compared to NiZr ³⁵.

In isotropic diffusion the atomic displacements are Gaussian distributed. In undercooled liquids and in glasses Gaussianity is violated over long time scales. This non-Gaussianity indicates different mobilities of different atoms over long time scales. This so called dynamic heterogeneity is quantified by the non-Gaussianity parameter³⁶

$$\alpha_2(t) = \frac{3 \langle \Delta r^4(t) \rangle}{5 \langle \Delta r^2(t) \rangle^2} - 1, \quad (6)$$

where $\langle \dots \rangle$ denotes time averaging and $\Delta r^2(t)$ and $\Delta r^4(t)$ are the mean square and quartic displacements.

Fig. 5 shows this non-Gaussianity in the Cu-subsystem for temperatures from 800 to 2000 K. The general behavior resembles the one observed in other glass formers. In the liquid above 1400 K dynamic heterogeneity is weak and due to different local vibrational densities of state. The maximal non-Gaussianity is at typical vibrational times (ps). With increasing undercooling and even more in the glassy state the non-Gaussianity rapidly increases. The maximum is reached later and later. Comparing with Fig. 3, one sees that the decay of the non-Gaussianity correlates with the onset of the diffusional part of the msqd following the plateau. The increase of $\alpha_2(t)$ from its vibrational value follows the \sqrt{t} law which was attributed to collective jump motion¹⁷.

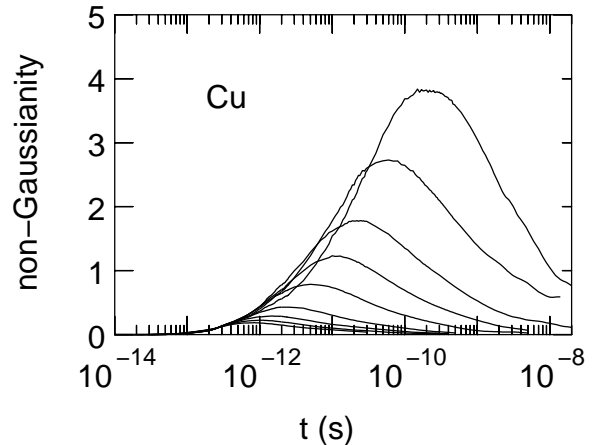


FIG. 5: Non-Gaussianity versus time of the Cu-subsystem in $\text{Zr}_{67}\text{Cu}_{33}$ on a logarithmic scale. Temperatures from top to bottom: 800, 900, 1000, 1100, 1200, 1400, 1600, 1800 and 2000 K.

V. JUMP LENGTH DISTRIBUTION

After aging we started the observation of jump processes. To get sufficient statistics we used observation times for the detection of jumps from 1.25 ns at 1400 K to 2.5 ns below 1200 K. As definition of jump we use a rapid transit of an atom between two sites of residence. One can see from a direct inspection of the particle trajectories that in dense liquids or glasses such “jumps” are not ballistic. For the CuZr system such a trajectory has been shown for a jump of a Cu-atom over a nearest neighbor distance in Refs. [33,37]. Furthermore the amplitudes of short time excursions are very large which makes an unambiguous definition of jumps difficult.

One method to detect atomic jumps is to study the “inherent dynamics” by quenching the system at given time intervals “instantaneously” to 0 K and then study the properties of the “energy landscape”. Here we use a more direct approach and define jumps by differences between atomic positions averaged over vibrational times. This means we define jumps of an atom in terms of absolute coordinates and not relative to the neighbors of the atom.

As a first step we define for each time step and each atom an average atomic position by

$$\langle \mathbf{R}^n(t) \rangle = \frac{1}{\delta_1} \int_{t-0.5\delta_1}^{t+0.5\delta_1} \mathbf{R}^n(t') dt'. \quad (7)$$

Since this averaging is done for each time step $\langle \mathbf{R}^n(t) \rangle$ is still, on the scale of the discretization by the simulation time step, a continuous function but is smoothed by averaging over the vibrations. An instantaneous jump would cause a steep ramp in $\langle \mathbf{R}^n(t) \rangle$.

For the detection of a jump we use two criteria. First, the instantaneous position of an atom must differ by a minimum cutoff length from the average taken at a pre-

vious time:

$$\left| \mathbf{R}(t) - \left\langle \mathbf{R}^n \left(t - \frac{1}{2} \delta \right) \right\rangle \right| > r_1. \quad (8)$$

We want to exclude from our jump detection those excursions where an atom has a large amplitude momentarily, but immediately returns to its old site. Therefore, when the above condition is fulfilled we additionally compare average positions separated by the fixed time interval δ_2

$$\Delta \langle \mathbf{R}^n(t) \rangle = \langle \mathbf{R}^n(t + 0.5\delta_2) \rangle - \langle \mathbf{R}^n(t - 0.5\delta_2) \rangle. \quad (9)$$

A jump at time t_0 is recorded when this difference for the first time exceeds a limit r_2

$$|\Delta \langle \mathbf{R}^n(t_0) \rangle| > r_2. \quad (10)$$

The corresponding atomic jump length is defined as

$$\ell = \Delta \langle \mathbf{R}^n(t_0) \rangle. \quad (11)$$

The time interval between the start time of the averaging for the final configuration, $t + 0.5\delta_2 - 0.5\delta_1$, and the end time of the averaging for the initial configuration, $t - 0.5\delta_2 + 0.5\delta_1$ is

$$t_{\text{wait}} = \delta_2 - \delta_1. \quad (12)$$

This method is rather CPU-time consuming since at each time step two averages have to be done for each atom. This is however necessary if one wants to get the necessary time resolution.

Throughout the simulation we used the parameters $\delta_1 = 2.5$ ps, $\delta_2 = 4$ ps and $r_2 = 0.05$ nm.

The necessity of averaging the atomic configurations over given time intervals limits the accuracy of the method. If a jump is completed in the time interval, t_{wait} , its length will be measured correctly by Eq. 9. A longer “jump time” leads to a reduced apparent jump length. On the other hand a movement of the atom with constant velocity v during the time $\delta_1 + \delta_2$ would be detected as jump if $v \cdot (\delta_1 + \delta_2) > r_2$. Since averaging over typical vibrational times implies $\delta_1 \sim$ ps we do not expect this to be an important limitation.

More serious is the limited resolution of rapid successive jumps. If two successive jumps are completed within the time interval t_{wait} they will be regarded as a single jump. If, however, the second jump happens near the end of the time interval it will be counted only partially. For example, should the second jump be the reverse of the first jump we might under some circumstances still record some shorter range jump, given by the sum of the forward jump and a fraction of the back-jump. On the other hand, if the first jump is rapidly followed by a successive forward jump, normally correlated with the first jump, we record an effective jump length which is too short. These two effects should approximately cancel for the investigated temperatures. For lower temperatures where the fraction of back-jumps increases it leads to an

overestimate of the mean square displacement calculated from the jumps, compared to the exact value.

Once the jump criteria hold for a time step they will normally hold for a subsequent time interval. To avoid double counting, therefore after each jump, we introduce a dead time δ_2 during which jumps are not counted. This will lead to small inaccuracies, mainly for the shortest jump lengths.

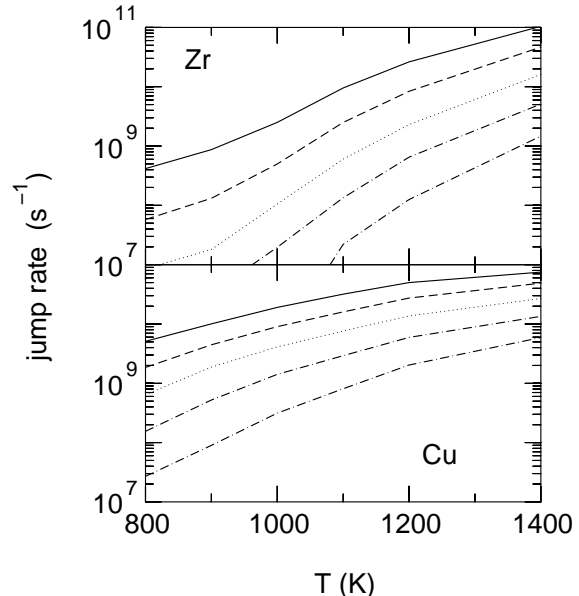


FIG. 6: Atomic jump rates, $\gamma_{\text{jump}}^j(\ell_{\text{cut}})$, on a logarithmic scale over temperature for Zr for different cutoff lengths, ℓ_{cut} : Zr (top) and Cu (bottom). Lines from top to bottom: $\ell_{\text{cut}} = 0.06, 0.1, 0.15, 0.2, 0.25$ nm.

From the recorded jumps we can calculate how often and how far each atom jumped during the observation time. This defines the average atomic jump rates

$$\gamma_{\text{jump}}^j(\ell_{\text{cut}}) = \frac{1}{N^j t_{\text{obs}}} \sum_{\ell < \ell_{\text{cut}}} N_{\text{jump}}^j(T, \ell, t_{\text{obs}}) \quad (13)$$

where $N_{\text{jump}}^j(T, \ell, t_{\text{obs}})$ is the number of jumps of atoms of species j with jump length in the interval $[\ell - \delta\ell/2, \ell + \delta\ell/2]$ with t_{obs} and T the observation time and temperature, respectively. Fig. 6 shows the rates for both components versus temperature for different cutoff length, $\ell \leq \ell_{\text{cut}}$. As to be expected the jump rates increase with temperature. No obvious break is apparent at T_c or T_g . For the lower temperatures the jump rate for Zr is clearly much smaller than that for Cu, particularly for the larger ℓ_{cut} . This is in accordance with the lower diffusivity of Zr. Jumps over nearest neighbor distances are observable for Zr only well above T_g . For Cu they are observed at all temperatures down to 800 K. At the highest temperature the rate for all jumps with $\ell \leq \ell_{\text{cut}} = 0.06$ nm approaches the theoretical limit of resolution of this simulation, $t_{\text{wait}}^{-1} = 2.5 \cdot 10^{11} \text{ s}^{-1}$. This limits the applicability of the method to higher temperatures. It reflects the

gradual transition from jumps to flow. It becomes meaningless to assign average starting positions to the atoms. In Fig. 6 average jump rates are shown. Individual atoms will have higher rates. However, the dynamic heterogeneity is no longer so important at $T = 1400$ K so that the deviations from the average are not too large. We will argue further down that the majority of apparent jumps with short lengths is actually due to the elastic displacement of surrounding atoms, accompanying all jumps.

For a more detailed investigation, we recorded for each detected jump the time of the jump and the initial and final positions of the jumping atom, according to Eq. 7. From these data the probability that an atom jumps by a certain distance is calculated. Summing over the atomic jumps we also calculate the atomic mean square displacements which can be compared with the ones gained directly in the simulation.

The probability that an atom jumps over a distance ℓ is

$$P^j(T, \ell) \delta \ell = \frac{1}{N^j t_{\text{obs}}} N_{\text{jump}}^j(T, \ell, t_{\text{obs}}). \quad (14)$$

Fig. 7 shows the distribution of the numbers of jumps per second against jump length for the larger majority component Zr for temperatures ranging from 900 to 1400 K (top) and for the smaller minority component Cu for temperatures ranging from 800 to 1400 K (bottom). Looking first at the curves for Zr one clearly sees no indication of a preferred jump length. The distribution can be fitted with a simple form

$$P_{\text{jump}}(T, \ell) = A_{\text{jump}} e^{-E_{\text{jump}}/kT} e^{-\ell/\ell_{\text{jump}}} \quad (15)$$

with $A_{\text{jump}}^{\text{Zr}} = 1.83 \cdot 10^{28}$ 1/(m·s), $E_{\text{jump}}^{\text{Zr}} = 1.51$ eV and $\ell_{\text{jump}}^{\text{Zr}} = 0.033$ nm. The apparent activation energy $E_{\text{jump}}^{\text{Zr}}$ agrees within some 10% with the diffusional one in the glassy state. In the expression for the undercooled melt, Eq. 4, it corresponds to the apparent activation energy at 1140 K. As shown by the dotted line this fit works well in the whole temperature range investigated which spreads over both T_g and T_c . Of course $E_{\text{jump}}^{\text{Zr}}$ has to be interpreted as an effective activation energy. There will be a spread of activation energies which is absorbed by the prefactor $A_{\text{jump}}^{\text{Zr}}$. The probability of jumps over a nearest neighbor distance is two orders of magnitude less than the one for jumps over half that distance.

In the case of Cu the situation seems more complicated. The probability of jumps over a nearest neighbor distance is only one order of magnitude less than the one for jumps over half that distance. Different from Zr, there is a distinct tail to higher jump lengths whose origin is not absolutely clear. One would expect a cutoff of $\Delta\langle \mathbf{R}^n(t) \rangle$ for distances not much greater than the nearest neighbor distance. In a densely packed material a jump over larger distances is highly improbable. We rather think that the tail is due to jumps which follow so rapidly that we cannot resolve them. This view is supported also by the correlation factors exceeding unity. We will see below

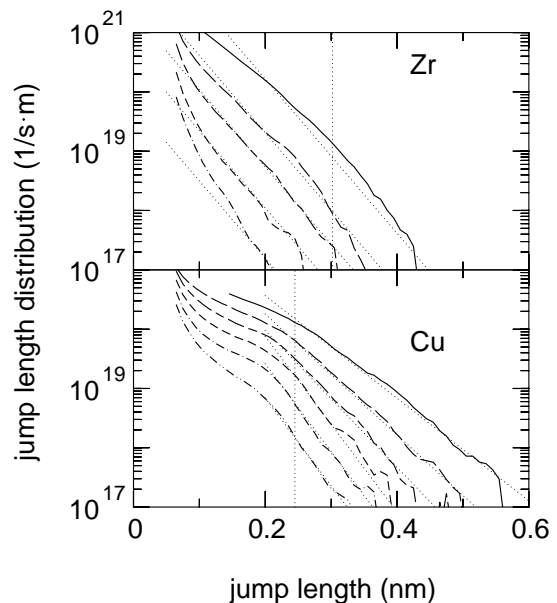


FIG. 7: Distribution of jumps/second over jump length for Zr (top) and Cu (bottom). Temperatures from top to bottom: 1400, 1200, 1100, 1000 and 900 K. The dotted lines indicate the fits by exponential jump length distributions, see text. The respective nearest neighbor distances for the two components are indicated by the vertical dotted lines.

that the contribution of these “extra long jumps” drops at T_c to less than 20% of the total atomic mean square displacement.

For short jump distances we see again the “elastic tail” which evolves into a shoulder before it merges with the curve for the more important long jumps. For these different fitting laws apply in the glass and in the undercooled liquid. In the glass, the Arrhenius form, Eq. 15, works just as for Zr. The fitted values are: $A_{\text{longjump}}^{\text{Cu}} = 9.79 \cdot 10^{26}$ 1/(s·m), $E_{\text{longjump}}^{\text{Cu}} = 0.82$ eV and $\ell_{\text{longjump}}^{\text{Cu}} = 0.024$ nm. This apparent activation energy is about 15% less than the diffusional E^m used in Fig. 4 but is higher than the value gained after including $T = 800$ K in the fit of the diffusivity.

This fit breaks down in the undercooled liquid regime. The slopes of the curves in Fig. 7 decrease with temperature, at variance with Eq. 15. Extending the fit from the glass into the liquid one finds still quite good values for jumps over nearest neighbor distances. However for $\ell = 0.4$ nm at $T = 1400$ K, Eq. 15 already underestimates the jump probability by nearly an order of magnitude. The jump length distribution for Cu in the undercooled liquid can be fitted by an exponential law with a temperature dependent $\ell_{\text{longjump}}(T)$

$$P_{\text{longjump}}^{\text{Cu}}(T, \ell) = B_{\text{longjump}}^{\text{Cu}} e^{-\ell/\ell_{\text{longjump}}(T)} \quad T > T_c \quad (16)$$

with $B_{\text{longjump}}^{\text{Cu}} = 1.96 \cdot 10^{22}$ 1/sm and $\ell_{\text{longjump}}(T) = 0.038, 0.043$ and 0.05 nm for $T = 1100, 1200$ and 1400 K, respectively. No direct physical origin for this relation is

evident. From the fact that the Arrhenius like temperature dependence, Eq. 15, is still applicable for jumps over nearest neighbor distances the most probable explanation seems to be that with increasing temperature more and more rapidly succeeding jumps, which cannot be resolved into separate single jumps, occur with predominantly additive direction. This is in accordance with the increase in correlation factor discussed later on in this paper.

For both components we observe a rapid increase of the jump length distribution toward short jump length. There is a clear excess above the value given by Eq. 15. For Zr at $T = 900$ K, where the feature is most prominent, it can be fitted by $P_{\text{jump}}(T, \ell) \propto 1/\ell^5$, close to the $\propto 1/\ell^4$ -dependence following from the $1/r$ decay of elastic displacements. We therefore conclude that this rapid increase reflects the elastic displacements accompanying all jumps. Due to dense packing they will also be present in the melt but are much more prominent in the glassy state. Two effects will strongly reduce their contribution to diffusion. First, the elastic displacement patterns are different for each jump leading to a cancellation of the bulk of these displacements after a few jumps. In the present system this is clearly observed in the glass when the Cu-atoms are by more than an order of magnitude more mobile than the Zr ones. The Cu-atoms move in a sluggish matrix of Zr-atoms. Jumps of the Cu-atoms will be accompanied by displacements of the Zr-atoms without destroying their topology. After a few subsequent jumps, dominated by the faster Cu, the Zr will more or less be back to their original sites. Our algorithm will pick up the occasional large displacements of the Zr but not their return in smaller steps. We will see this effect, further down, in the mean square displacement of Zr at $T \leq 900$ K, Fig. 10. temperatures the dynamic heterogeneity, meaning that at any given time only a small subset of atoms is mobile, will increase this effect and spread it to the second component. Secondly, after a jump process the glass is locally excited and relaxes toward the local equilibrium. This is done by comparatively slight shifts of the average atomic positions. This again reduces the contribution of the small lengths to diffusion.

VI. AVERAGE MEAN SQUARE DISPLACEMENTS

To check the importance of the different jump lengths for diffusion we compare the average atomic mean square displacement (msqd) taken directly from MD with the one obtained by adding the jumps used to obtain the distribution of Fig. 7:

$$|\Delta R_{\text{jump}}(t, \ell_{\text{cut}})|^2 = \langle \left| \sum_{\substack{t' < t \\ \Delta R^n > \ell_{\text{cut}}}} \Delta \mathbf{R}^n(t') \right|^2 \rangle_n \quad (17)$$

where $\langle \dots \rangle_n$ indicates averaging over atoms and configurations. We do this for different lower cutoffs of the jump length, ℓ_{cut} . In the undercooled melt, Figs. 8 and 9, there

is an excellent agreement between the exact curves and the ones gained this way. In the figures, we added to $|\Delta R_{\text{jump}}^n(t, \ell_{\text{cut}})|^2$ the vibrational msqd which can be obtained from the short time behavior.

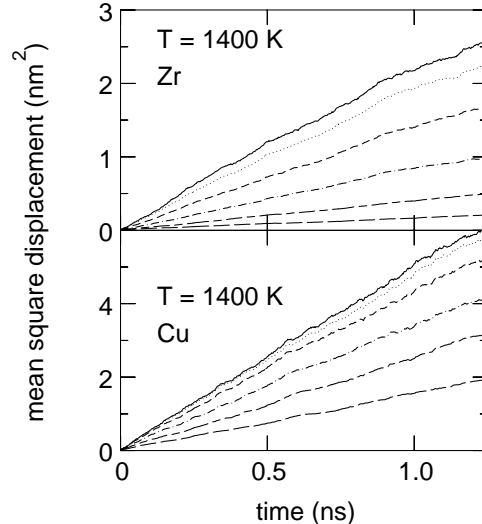


FIG. 8: Average atomic mean square displacement versus time at $T = 1400$ K (full line). Atomic mean square displacement calculated from the jumps used for the distribution, Fig. 1, for different cutoffs: from top to bottom all jumps with jump lengths greater than 0.06, 0.1, 0.15, 0.2 and 0.25 nm.

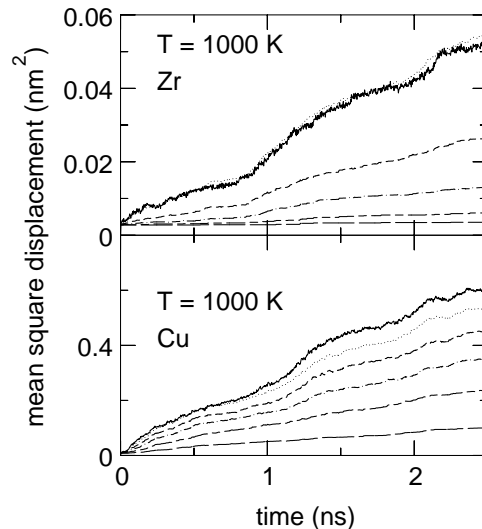


FIG. 9: Average atomic mean square displacement versus time at $T = 1000$ K (full line). Atomic mean square displacement calculated from the jumps used for the distribution, Fig. 1, for different cutoffs: from top to bottom all jumps with jump lengths greater than 0.06, 0.1, 0.15, 0.2 and 0.25 nm.

We find for Zr that even at the temperature $T = 1400$ K, i.e. about 40% above T_c , the msqd and, therefore also diffusion, is dominated by jumps much shorter than the nearest neighbor distance, $R_{NN}^{\text{Zr}} \approx 0.3$ nm.

Jumps of more than 0.25 nm contribute about 5%. At $T = 1000$ K their contribution vanishes. In Cu, jumps over $R_{NN}^{\text{Cu}} \approx 0.25$ nm give at $T = 1400$ K about a quarter of the msqd. At $T = 1000$ K this contribution is diminished to 10%. This means that at $T = T_c$ short jumps dominate the diffusion of both components.

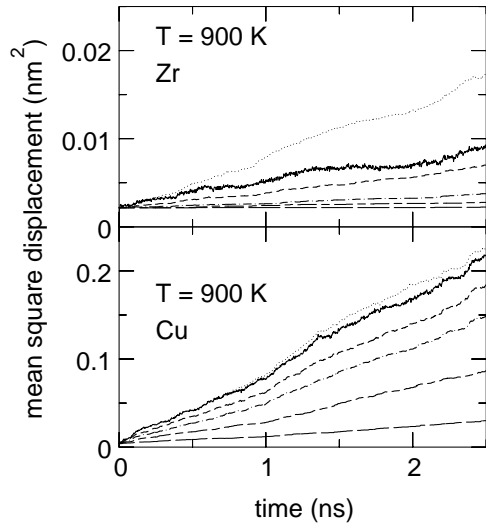


FIG. 10: Average atomic mean square displacement versus time at $T = 900$ K (full line). Atomic mean square displacement calculated from the jumps used for the distribution, Fig. 1, for different cutoffs: from top to bottom all jumps with jump lengths greater than 0.06, 0.1, 0.15, 0.2 and 0.25 nm.

At $T = 900$ K, in the glass, the situation is similar for Cu. For Zr the contribution of long jumps is nearly negligible. The contribution of short jumps, $\ell < 0.1$ nm and particularly $\ell < 0.06$ nm (dashed and dotted lines in Fig. 10), is severely overestimated. This can be traced to the “elastic displacements” discussed in the previous section. The motion of the Cu-atoms in the Zr matrix causes displacements of the latter. Since the Zr subsystem is sluggish compared with that of Cu, it has some memory over several jumps of the Cu system. Zr-atoms will have a preference to return to their original site. Or speaking in terms of potential energy, the system can be approximated for some time as being in a minimum with the Cu motion as perturbation. The Zr-atoms remain in their “cages” over many “cage-escapes” of the Cu-atoms. While the Zr is in its cage it will occasionally perform jumps picked up by the algorithm, followed by several short jumps, not picked up. This can be seen by monitoring the motion of the single atoms. An indication of this effect can be seen in Fig. 10 where, for Zr, the dotted curve initially follows the real msqd (full line) but later rises also when the real msqd of Zr stays more or less constant while the msqd of Cu increases. This is the discussed effect of Zr-atoms temporarily being displaced by Cu-jumps and their return in several smaller steps not being detected. In this sense the “surplus” of detected Zr-jumps corresponds to an in-cage motion.

We argued above that the rapid increase of $P^j(T, \ell)$ for $\ell \rightarrow 0$ is due to elastic displacements, i.e. displacements caused in the matrix when an atom or a group of atoms jumps, and that these displacements will not contribute strongly to diffusion. As diffusion drops with sinking temperature, the ratio of probability of these non diffusive “jumps” over the one given by Eq. 15 rises strongly, see Fig. 6. If one does a simple correction of the curves for the two smaller cutoffs ($\ell_{\text{cutt}} = 0.06$ and 0.1 nm) by this ratio, the excess is removed and the msqd is actually underestimated by 30%. Such a simple correction does, of course, not distinguish between “in cage” and “out of cage jumps”. These “non-diffusive short range jumps” exist also in lattices. A jump of an atom into a neighboring vacancy site causes displacements of the surrounding atoms which will disappear again when the vacancy moves on. In lattices these can easily be measured and accounted for by means of lattice geometry and symmetry. In an amorphous material this is no longer possible and it becomes only a posteriori clear which of the short range displacements contribute to diffusion and which are non-diffusive.

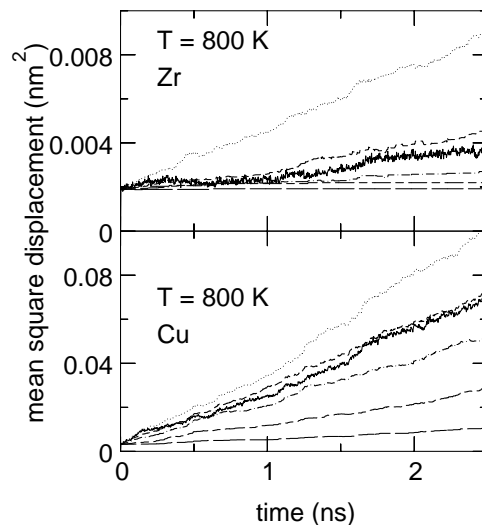


FIG. 11: Average atomic mean square displacement versus time at $T = 800$ K (full line). Atomic mean square displacement calculated from the jumps used for the distribution, Fig. 1, for different cutoffs: from top to bottom all jumps with jump lengths greater than 0.06, 0.1, 0.15, 0.2 and 0.25 nm.

Decreasing the temperature to 800 K the contribution of these elastic or “in cage” jumps increases further and becomes visible also for the more mobile Cu-atoms, Fig. 11. This can be attributed to the increasing dynamic heterogeneity. Like most of the Zr-atoms, an increasing number of Cu-atoms becomes immobile on the time scale of several jumps. The Cu-atoms, mobile at a given time, move in a matrix of Zr- and immobile Cu-atoms which are temporarily displaced.

VII. CORRELATION FACTOR

In analogy to Eq. 17 we can define an “uncorrelated msqd” by

$$|\Delta R_{\text{uncorr}}(t, \ell_{\text{cut}})|^2 = \langle \sum_{\substack{t' < t \\ \Delta R^n > \ell_{\text{cut}}}} |\Delta \mathbf{R}^n(t')|^2 \rangle_n \quad (18)$$

and a correlation factor³⁸

$$f_{\text{corr}} = \lim_{t \rightarrow \infty} \frac{|\Delta R_{\text{jump}}^n(t, \ell_{\text{cut}})|^2}{|\Delta R_{\text{uncorr}}^n(t, \ell_{\text{cut}})|^2}. \quad (19)$$

Correlation factors have been studied in the past extensively for diffusion in lattices^{39,40}. If the jumps are completely uncorrelated (random walk) one has $f_{\text{corr}} = 1$. This would be the case for an isolated interstitial atom, e.g. H in Pd, moving between equivalent sites. For diffusion by a vacancy mechanism, neglecting lattice displacements, the correlation factor is reduced in simple lattices to $f_{\text{corr}} \approx 1 - 2/z$ where z is the number of nearest neighbors. The term $2/z$ accounts for the direct back-jumps of the tracer atom into the same vacancy. Exact calculations give for the vacancy mechanism in fcc lattices $f_{\text{corr}} = 0.78$, whereas for a diamond lattice one has $f_{\text{corr}} = 0.5$ due to the lower number of neighbors. In simple lattices the correlation factor is given by geometry alone and is temperature independent. In more complicated structures when more than one type of jump is involved the correlation factor becomes temperature dependent. An bias due to an external field increases the correlation factor.

If one would study self diffusion in a simple fcc lattice along the lines of the two preceding sections one would obtain two sets of jumps with two sets of correlation factors. “Diffusive jumps” would have a jump length of about a nearest neighbor distance and a correlation factor as discussed above. The short “non-diffusive jumps”, i. e. the temporary displacements due to the “diffusive jumps”, on the other hand, would have a correlation factor $f_{\text{corr}} = 0$. The total correlation factor is thus somewhat reduced from the rigid lattice value. Total correlation factors zero are observed in lattices when atoms jump between a finite number of sites, e. g. the cage motion of interstitial Co in Al⁴¹.

These general considerations assume that the diffusing particle is completely thermalized between jumps, i. e. that there are no memory effects. At temperatures near the melting point this is no longer the case. In simulations of vacancy diffusion in Al and Na lattices it was found, that when the waiting time between successive jumps shrinks to the order of vibrational time scales (ps), successive jumps become correlated, forward jumps become more frequent and, subsequently, the correlation factor for vacancy diffusion becomes larger than the random walk value, $f_{\text{corr}} > 1$ ^{40,42}.

Transferring these results to the amorphous and under-cooled liquid states, one expects to find total correlation

factors considerably smaller than 1 for diffusion via a vacancy type mechanism, and near to 1 for diffusion via an inherent mechanism as postulated in the review¹. The correlation factor for the longer jumps should be larger than for the shorter ones since the latter have a larger non-diffusive contribution. Cooling below T_g , the correlation factor should drop because more and more jump directions become blocked. Unfortunately, due to the computational limitations, this effect cannot be explored fully at present. In the liquid, where we have seen that the jump frequency becomes comparable to the vibration time, we expect an increase of the correlation factor with temperature.

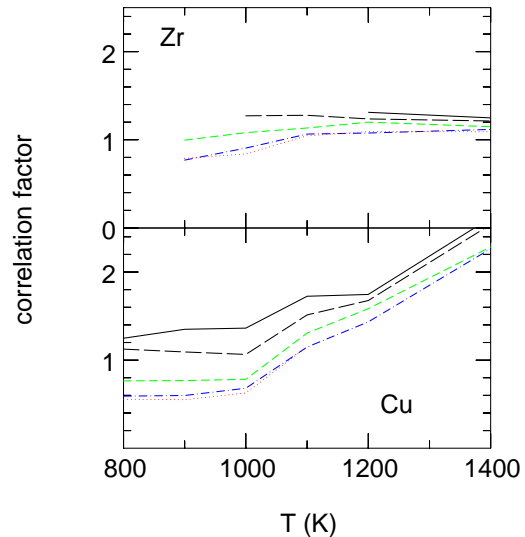


FIG. 12: Average atomic mean square displacement versus time at $T = 800$ K (full line). Atomic mean square displacement calculated from the jumps used for the distribution, Fig. 1, for different cutoffs: from top to bottom all jumps with jump lengths greater than 0.25, 0.20, 0.15, 0.1 and 0.06 nm.

The correlation factors calculated from the observed jumps are shown in Fig. 12. By their very construction immediately following jumps are excluded due to the dead time between jumps. The general trends are clearly seen in the Fig. The correlation factors for the long jumps are close to 1 or even larger, indicating diffusion by an inherent mechanism. The total correlation factor drops upon cooling which explains the drop of the diffusion constant below its Arrhenius line despite the seemingly constant effective activation energy for the jumps themselves. Striking is the increase of the correlation factor for Cu jumps to values around two for $T = 1400$. This will be an effect of insufficient thermalisation between jumps. It also indicates the transition from jump to flow motion. For the larger and heavier Zr-atoms this effect is strongly suppressed.

VIII. DISCUSSION

Upon quenching, the mean square displacements, in a log-log representation, show for both components of $\text{Cu}_{33}\text{Zr}_{67}$ the normal behavior of a transition from a hot liquid, via an undercooled one, to a glass. Between the $\propto t^2$ behavior, indicating ballistic motion or vibrations, and the $\propto t$ regime of diffusion a plateau develops. The diffusion dynamics can be described by the mode coupling scenario. However, the temperature dependences of the two components do not run as parallel as in the often used binary Lennard-Jones system either under constant volume⁴³ or constant pressure conditions¹⁹. Such a difference could be the origin of the order of magnitude difference between diffusivity of Ni and Ti and the one gained via the Einstein relation from the viscosity in ZrTiCuNiBe bulk glasses⁴⁴ which was, similarly to the present findings, explained by a faster diffusion of the smaller components in a relatively rigid Zr-matrix. This behavior seems to be typical for ZrCu systems. In a simulation of the binary NiZr system no such pronounced effect was found⁷.

Upon quenching, the dynamic heterogeneity rises rapidly above its vibrational value at temperatures below $T = 1400$ K which, in absence of a reliable estimate of the melting point of our system, we take as a rough indication of undercooling.

The distribution of the jump lengths of both components, both above and below T_c is a smooth function of distance, definitely excluding a preference of nearest neighbor jumps. Such a smooth distribution is to be expected for collective jumps as they are seen in the typical chain-like motion of metallic glasses^{8,9,11}. Using the energy landscape approach similar results were found for a binary Lennard-Jones system near T_c ⁴⁵ and were also attributed to cooperative motion which in that system would be additionally furthered by the inherent higher density. It is encouraging that the two different and complementary approaches lead to the same conclusion.

This result, of a missing typical jump length, will not be affected by the rapid quench inherent to simulations. Both experiment¹ and simulation of either activation volume¹⁹ or isotope effect⁴⁶ indicate that insufficient aging would, if anything, enhance the number of single particle jumps with their inherent length scale.

For the structure forming majority component Zr, the jump length distribution is given by the product of two terms, an Arrhenius term for the temperature dependence and a temperature independent distribution of jump lengths. An Arrhenius law for the temperature dependence, irrespective of the details of the barrier distribution has been derived earlier in an effective medium treatment of hopping in disordered materials⁴⁷. The spatial dependence shows a power law for short distances and an exponential one for the longer distances. This form is again in agreement with the findings of the energy landscape study⁴⁵. The power law part for short distances can be understood as being caused by the elastic

displacement accompanying any hopping process. These would be also seen for hopping in a lattice where, different from a disordered system, they can easily be identified from translational symmetry. They are largely reverted by subsequent hops and will not contribute markedly to long range diffusion. The exponential long distance dependence results, in our opinion, from the collectivity of the jumps. Jumps are closely correlated to low frequency quasi-localized vibrations⁴⁸. The cores of these show, similarly to the true localized vibrations, an exponential decay of the amplitudes⁴⁹.

The jump length distribution of the minority component, Cu, has qualitatively the same behavior, however, with one important difference. The Arrhenius scaling with temperature breaks down above T_c . The distribution is stretched to greater length and also the total number of long jumps is increased. We have related this to lacking thermalisation between jumps, a view supported by the correlation factors.

The correlation factors are of order unity. This is a signature of diffusion by an inherent mechanism, as opposed to a defect (quasi-vacancy) mediated one which would lead to clearly smaller correlation factors. The correlation factor of Cu for $T > T_c$ is an exception. It increases strongly with temperature. Such correlation factors > 1 are known to result when the time between jumps no longer allows for thermalisation. It indicates, in this respect, the transition from jump-like motion to flow.

From the contribution of the different jump length to the mean square displacements it is obvious that long distance jumps only play a minor role in Zr diffusion. Their role is greater for Cu where at T_c jumps over more than 0.2 nm contribute more than 30%. From direct inspection of individual jumps one sees, that in the usual chain of collectively jumping atoms Cu-atoms will show the largest displacements. At the higher temperatures, often more than one Cu atom jumps over a nearest neighbor distance. The replacement chains observed in the early work^{5,6} are a special case of this scenario.

The absence of a preferred jump length might, *prima facie*, be taken as a contradiction to the time evolution of the van-Hove self correlation function where, in the undercooled liquid, clearly a secondary peak at the nearest neighbor distance evolves. One of the authors showed earlier for the same material that the time evolution of the van-Hove self correlation function for Cu near $T = T_c$ can be reproduced by a model comprising only nearest neighbor jumps and a residue of short distance jumps, called flow-like motion¹⁶. For Cu an apparent activation energy of 850 meV, in good agreement with the present value of 820 meV, was given. Combining this and the present results one can conclude that the secondary peak in the van-Hove function indicates preferred resting positions for the Cu-atoms in the Zr-matrix which is rigid on the time scale of the Cu diffusion. A similar conclusion was arrived at for the Lennard-Jones system from the energy landscape picture^{45,50} when the dynamic

heterogeneity creates a sufficiently rigid matrix of immobile particles. Diffusion becomes dominated by transitions between these minima, a connected network of minima is formed^{51,52,53} or “coarse graining” occurs⁵⁴. The strongly different diffusivities of the present system enhance the effect and are an additional source of “metabasins”⁵⁵. The diffusion of the Cu in the deeply undercooled liquid and even more in the glass has features of a diffusion between “traps”.

In the previous work¹⁶, as the temperature is lowered, an increase in jump reversal was reported. This is compatible with the reported correlation factors of the present work. A relative increase of reversible jumps for lower temperatures has also been observed from a jump analysis of the binary Lennard-Jones system below T_c ⁵⁶.

IX. SUMMARY

In summary we calculated the diffusion of Cu and Zr above and below the glass transition temperature. Different to the commonly studied Lennard-Jones system Cu shows in the undercooled liquid a strongly enhanced diffusivity, compared to the majority component Zr. We think that this effect is related to the weaker coupling between the two components in the present system which is seen also in the reduced enthalpy of fusion.

The distribution of atomic jumps in the liquid and glassy state can be described by simple exponential dependencies on jump length and temperature. There is a smooth transition from flow to hopping. For the faster Cu this is reflected in the undercooled liquid by correlation factors exceeding unity, indicating a breakdown of thermalisation between jumps. We find no preferred jump length around the nearest neighbor distance. The observed secondary peaks in the van-Hove function are, therefore, clearly not an effect of the jumps directly but of increased waiting times at given sites. This effect will be enhanced by the growth of the dynamical heterogeneity upon cooling. On the time scale of the inverse of the jump frequency of the mobile atoms, more and more atoms are immobile and provide a semi rigid background thus creating preferred sites. The effect is seen more strongly by the smaller atoms (Cu).

APPENDIX A: MODIFIED EMBEDDED ATOM INTERACTION (MEAM)

We use the MEAM model developed for the CuZr system by Gaukel²⁷. For completeness we give below the analytic form and the parameters.

In the Embedded Atom Method (EAM) model⁵⁷ the interatomic interaction is described by pair potential Φ_{two} and an embedding energy $F_{\text{ea}}(\rho)$ which accounts for the additional many body effects due to the electronic

density:

$$E_{\text{pot}} = \sum_{\substack{m,n=1 \\ m \neq n}}^N \frac{1}{2} \Phi_{\text{two}}^{\ell^m \ell^n} (R^{mn}) + \sum_{n=1}^N F_{\text{ea}}^{\ell^n} (\rho(\mathbf{R}^n)) \quad (\text{A1})$$

where $R^{mn} = |\mathbf{R}^m - \mathbf{R}^n|$ is the distance between atoms m and n , and ℓ^n indicates the type of atom, in our case Zr or Cu.

For the pair potential we use the analytic form

$$\begin{aligned} \Phi_{\text{two}}(R^{mn}) = & c_1 e^{-c_2 R^{mn}} + c_3 e^{-c_4 (R^{mn} - R_0)^2} \\ & + c_5 (R^{mn})^6 + c_6 (R^{mn})^7 + c_7 \quad (\text{A2}) \end{aligned}$$

The small parameters c_5 , c_6 and c_7 are given by the condition that Φ_{two} and its first two derivatives vanish at R_{cutoff} . The parameters are given in Table I for Zr and Cu. For the mixed interaction we use the the mean

$$\Phi_{\text{two}}^{\text{ZrCu}}(R^{mn}) = (\Phi_{\text{two}}^{\text{ZrZr}}(R^{mn}) + \Phi_{\text{two}}^{\text{CuCu}}(R^{mn})) / 2. \quad (\text{A3})$$

	Zr	Cu
c_1 [eV]	$3.457155 \cdot 10^4$	$6.547955 \cdot 10^5$
c_2	4.479563	6.487234
c_3 [eV]	-1.062312	-2.383022
c_4	0.8614267	0.1318588
R_0 [Å]	2.952510	0.6049550
c_5 [eV/Å ⁶]	$-4.971823 \cdot 10^{-8}$	$-3.085439 \cdot 10^{-4}$
c_6 [eV/Å ⁷]	$6.337047 \cdot 10^{-9}$	$5.310256 \cdot 10^{-5}$
c_7 [eV]	$6.636436 \cdot 10^{-4}$	0.9001767
R_{cutoff} [Å]	6.57620462	4.44761582

TABLE I: The constants of the pair potential, Eq. A2.

For the embedding term, we use the form proposed by Baskes⁵⁸ for both components

$$F_{\text{ea}}(\rho(\mathbf{R}^n)) = c_1 \rho(\mathbf{R}^n) \cdot \ln(c_2 \rho(\mathbf{R}^n)) \quad (\text{A4})$$

with the parameters given in Table II.

	Zr	Cu
c_1 [eV · Å ³]	2.71082977	2.02891465
c_2 [Å ³]	0.737740301	0.876399217

TABLE II: The constants used in the embedding term, Eq. A4.

In the original EAM, the density ρ in Eq. A1 and Eq. A4 is given as a superposition of radial functions

$$\rho_0(\mathbf{R}^n) = \sum_{\substack{m=1 \\ m \neq n}}^N f(R^{mn}). \quad (\text{A5})$$

For the function $f(R^{mn})$ we use an exponential plus additional terms to set the function and its first two derivatives to zero at the cutoff.

$$f(R^{mn}) = c_1 e^{-c_2 R^{mn}} + c_3 (R^{mn})^{c_4} + c_5 (R^{mn})^{c_4+1} + c_6 \quad (\text{A6})$$

The parameters are compiled in Table. III

		Zr	Cu
c_1	$1/\text{\AA}^3$	1.04537268	0.896989894
c_2		0.123135389	0.286315587
c_3	$1/\text{\AA}^3$	$5.54697310 \cdot 10^{-12}$	$6.74032288 \cdot 10^{-6}$
c_4		15.1751328	7.51090487
c_5	$1/\text{\AA}^3$	$-9.43929033 \cdot 10^{-13}$	$-1.22957801 \cdot 10^{-6}$
c_6	$1/\text{\AA}^3$	-0.597896189	-0.345100552
R_{cutoff}	$[\text{\AA}]$	5.16447906	4.28405051

TABLE III: Parameters of the spherical density function, Eq. A6.

In the MEAM additional angular terms are added to allow for covalent effects⁵⁸ needed to describe non ideal hcp lattices. We restrict ourselves to terms in the third power of the cosine of the apex angle

$$\cos(\Theta^{mnl}) = \left(\frac{\mathbf{R}^{mn} \mathbf{R}^{ln}}{R^{mn} R^{ln}} \right).$$

The density then takes the form

$$\rho(\mathbf{R}^n) = \rho_0(\mathbf{R}^n) \exp \left[\frac{1}{(\rho_0(\mathbf{R}^n))^2} c_3 \times \sum_{\substack{l,m=1 \\ l \neq n \\ m \neq n}}^N \cos^3(\Theta^{mnl}) f_3^{\ell^m}(R^{mn}) f_3^{\ell^l}(R^{ln}) \right]. \quad (\text{A7})$$

The angular correction in the MEAM is only needed for Zr as apex atom but not for Cu. We, therefore, put $c_3 = 0$ for Cu, Table IV

For the radial function in the angular correction term we used the same form as for the spherical part

$$f_3(R^{mn}) = c_1 e^{-c_2 R^{mn}} + c_3 (R^{mn})^{c_4} + c_5 (R^{mn})^{c_4+1} + c_6 \quad (\text{A8})$$

with the parameters given in Table V.

- ¹ F. Faupel, W. Frank, M.-P. Macht, H. Mehrer, V. Naundorf, K. Rätzke, S. K. Sharma, H. R. Schober, and H. Teichler, *Rev. Mod. Phys.* **75**, 237 (2003).
- ² W. Götze and A. Sjölander, *Rep. Prog. Phys.* **55**, 241 (1992).
- ³ H. Ehmler, A. Heesemann, K. Rätzke, F. Faupel, and U. Geyer, *Phys. Rev. Lett.* **80**, 4919 (1998).
- ⁴ F. Faupel, P. W. Hüppe, and K. Rätzke, *Phys. Rev. Lett.* **65**, 1219 (1990).
- ⁵ H. Miyagawa, Y. Hiwatari, B. Bernu, and J. Hansen, *J. Chem. Phys.* **88**, 3879 (1988).
- ⁶ G. Wahnström, *Phys. Rev. A* **44**, 3752 (1991).
- ⁷ H. Teichler, *Defect and Diffusion Forum* **143-147**, 717 (1997).
- ⁸ H. R. Schober, C. Gaukel, and C. Oligschleger, *Defect and Diffusion Forum* **143-147**, 723 (1997).
- ⁹ C. Donati, J. F. Douglas, W. Kob, S. J. Plimpton, P. H. Poole, and S. C. Glotzer, *Phys. Rev. Lett.* **80**, 2338 (1998).
- ¹⁰ H. Teichler, *J. Non-Cryst. Solids* **293-295**, 339 (2001).
- ¹¹ H. R. Schober, C. Oligschleger, and B. B. Laird, *J. Non-Cryst. Sol.* **156**, 965 (1993).
- ¹² W. Frank, A. Hörner, P. Scharwaechter, and K. Kronmüller, *Mat. Science Eng.* **A179/A180**, 36 (1994).
- ¹³ L. D. V. Ee, B. J. Thijsse, and J. Sietsma, *J. Non-Cryst. Solids* **205-207**, 641 (1996).

		Zr	Cu
c_3		-5.36035659	0

TABLE IV: Parameters of the angular correction in the MEAM, Eq. A7.

- ¹⁴ J. Roux, J. Barrat, and J.-P. Hansen, *J. Phys.: CM* **1**, 7171 (1989).
- ¹⁵ T. B. Schröder and J. C. Dyre, *J. Non-Cryst. Solids* **235-237**, 331 (1998).
- ¹⁶ C. Gaukel and H. R. Schober, *Solid State Commun.* **107**, 1 (1998).
- ¹⁷ D. Caprion, J. Matsui, and H. R. Schober, *Phys. Rev. Lett.* **85**, 4293 (2000).
- ¹⁸ K. Vollmayr-Lee, W. Kob, K. Binder, and A. Zippelius, *J. Chem. Phys.* **116**, 5158 (2002).
- ¹⁹ H. R. Schober, *Phys. Rev. Lett.* **88**, 145901 (2002).
- ²⁰ M. I. Baskes and R. A. Johnson, *Modelling Simul. Mater. Sci. Eng.* **2**, 147 (1994).
- ²¹ J. H. Rose, J. R. Smith, F. Guinea, and J. Ferrante, *Phys. Rev. B* **29**, 2963 (1984).
- ²² E. Kneller, Y. Khan, and U. Gorres, *Z. Metallkd.* **77**, 43 (1986).

		Zr	Cu
c_1	$1/\text{\AA}^3$	1.04537268	0.896989891
c_2		0.146268549	1.0000000
c_3	$1/\text{\AA}^3$	$2.37968067 \cdot 10^{-14}$	$2.67398161 \cdot 10^{-5}$
c_4		19.5094567	6.00000000
c_5	$1/\text{\AA}^3$	$-4.53181412 \cdot 10^{-15}$	$-5.15696452 \cdot 10^{-6}$
c_6	$1/\text{\AA}^3$	-0.57983725	$-4.14635228 \cdot 10^{-2}$
R_{cutoff}	$[\text{\AA}]$	4.74779381	4.0000000

TABLE V: Parameters of the angular density function, Eq. A8.

- ²³ A. I. Zaitsev and N. E. Zaitseva, High Temperature **41**, 49 (2003).
- ²⁴ P. Ehrhart, in *Atomic Defects in Metals*, edited by H. Ulm-maier (Springer, Berlin, 1999), vol. 25 of *Landolt-Börnstein New Series III*, p. 32.
- ²⁵ F. Willaime and C. Massobrio, PRL **63**, 2244 (1989).
- ²⁶ B. L. Zhang, C. Z. Wang, K. M. Ho, D. Turner, and Y. Y. Ye, Phys. Rev. Lett. **74**, 1375 (1995).
- ²⁷ C. Gaukel, *Dynamics of Glasses and Undercooled Melts of Zr-Cu*, vol. 3556 of *Berichte des Forschungszentrums Jülich* (Forschungszentrum Jülich, Germany, 1998).
- ²⁸ M. Parrinello and A. Rahman, Phys. Rev. Lett. **45**, 1196 (1980).
- ²⁹ W. G. Hoover, Phys. Rev. A **31**, 1695 (1985).
- ³⁰ E. Kneller, C. Du, D. Dümpelmann, B. Fröchte, Y. Khan, and M. Sostarich, Z. Metallkd. **84**, 574 (1993).
- ³¹ H. N. Ritland, J. Am. Ceram. Soc. **37**, 370 (1954).
- ³² D. Caprion and H. R. Schober, J. Chem. Phys. **117**, 2814 (2002).
- ³³ M. Kluge, *Molekulardynamik-Simulation der Diffusion in binären unterkühlten metallischen Schmelzen und Gläsern aus Cu₃₃Zr₆₇*, vol. 3913 of *Berichte des Forschungszentrums Jülich* (Forschungszentrum Jülich, Germany, 2001).
- ³⁴ H. Teichler, Phys. Rev. Lett. **76**, 62 (1996).
- ³⁵ A. I. Zaitsev, N. E. Zaitseva, E. K. Shapkhazov, and A. A. Kodentsov, Phys. Chem. Chem. Phys. **4**, 6047 (2002).
- ³⁶ A. Rahman, Phys. Rev. **136**, A405 (1964).
- ³⁷ C. Gaukel, M. Kluge, and H. R. Schober, J. Non-Cryst. Sol. **250-252**, 664 (1999).
- ³⁸ A. R. Allnatt and A. B. Lidiard, Rep. Prog. Phys. **50**, 373 (1987).
- ³⁹ C. P. Flynn, *Point Defects and Diffusion* (Clarendon, Oxford, 1972).
- ⁴⁰ J. Philibert, *Atom movements, Diffusion and mass transport in solids* (Les Éditions de Physique, Les Ulis, France, 1991).
- ⁴¹ P. Ehrhart, K. H. Robrock, and H. R. Schober, in *Physics of Radiation Defects in Crystals*, edited by R. A. Johnson and A. N. Orlov (North-Holland, Amsterdam, 1986), p. 3.
- ⁴² C. H. Bennett, in *Diffusion in Solids, Recent Developments*, edited by A. S. Nowick and J. J. Burton (Academic Press, New York, 1975), p. 74.
- ⁴³ W. Kob and H. C. Andersen, Phys. Rev. E **51**, 4626 (1995).
- ⁴⁴ A. Meyer, W. Petry, M. Koza, and M.-P. Macht, Appl. Phys. Lett. **83**, 3894 (2003).
- ⁴⁵ T. B. Schröder, S. Sastry, J. C. Dyre, and S. C. Glotzer, J. Chem. Phys. **112**, 9834 (2000).
- ⁴⁶ H. R. Schober, Solid State Commun. **119**, 73 (2001).
- ⁴⁷ M. Wagener and W. Schirmacher, Ber. Bunsenges. Phys. Chem. **95**, 983 (1991).
- ⁴⁸ H. R. Schober and C. Oligschleger, Phys. Rev. B **53**, 11469 (1996).
- ⁴⁹ H. R. Schober and G. Ruocco, Phil. Mag. B **84**, 1361 (2004).
- ⁵⁰ S. Büchner and A. Heuer, Phys. Rev. Lett. **84**, 2168 (2000).
- ⁵¹ F. H. Stillinger, Science **267**, 1935 (1995).
- ⁵² L. Angelani, G. Parisi, G. Ruocco, and G. Vilianni, PRL **81**, 4648 (1998).
- ⁵³ M. Schulz, Phys. Rev. B **57**, 11319 (1998).
- ⁵⁴ B. Rinn, P. Maass, and J.-P. Bouchaud, PRB **64**, 104417 (2001).
- ⁵⁵ B. Doliwa and A. Heuer, Phys. Rev. E **67**, 030501(R) (2003).
- ⁵⁶ K. Vollmayr-Lee, J. Chem. Phys. **121**, 4781 (2003).
- ⁵⁷ M. S. Daw and M. I. Baskes, Phys. Rev. Lett. **50**, 1285 (1983).
- ⁵⁸ M. I. Baskes, Phys. Rev. Lett. **59**, 2666 (1987).